JPMTR-2016
DOI 10.14622/JPMTR-2016
UDC 667.5:777-023.8

Original scientific paper | 147
Received: 2020-12-05
Accepted: 2021-04-22

Ink splitting in gravure printing: localization of the transition from dots to fingers

Pauline Brumm[1,2], Tim Eike Weber[1], Hans Martin Sauer[1,2] and Edgar Dörsam[1,2]

[1] Technical University of Darmstadt, Department of Mechanical Engineering, Institute of Printing Science and Technology, Magdalenenstr. 2, 64289 Darmstadt, Germany
brumm@idd.tu-darmstadt.de
timweber@idd.tu-darmstadt.de
sauer@idd.tu-darmstadt.de

[2] Collaborative Research Center (CRC) 1194, Interaction between Transport and Wetting Processes, Project C01, Germany
doersam@idd.tu-darmstadt.de

Abstract

For the gravure printing process, ink transfer from the printing cylinder to the substrate is studied in the parameter regime at the very border between point and lamella splitting. In this parameter regime, ink drop deposition from adjacent gravure cells is such that, by capillary and wetting forces in the nip, the drops are at the onset of mutual coalescence. This process offers the possibility to deposit an ultimately thin and closed ink film. We discuss the particular type of pattern and defect formation in the printed layer and show that these apparently stochastic patterns have reproducible features. We claim that, besides the two known regimes of point and lamella splitting, at least one additional ink transfer regime is possible, with well-controllable wetting and ink flow dynamics. A classification scheme is proposed, based on raster-scale pattern phenomenology, by which the printer can recognize and distinguish this third regime by optical inspection of the printed product. Gaining control over this regime offers novel opportunities for gravure printing in thin-film related applications such as printed electronics and package printing.

Keywords: ink transfer, viscous fingering, Saffman-Taylor instability, functional printing, print quality

1. Introduction and background

Gravure printing technique is, amongst the various printing techniques, one of the most promising technologies for future printing applications beyond graphical arts (Kumar, 2015), for example, printed electronics (Ganz, et al., 2016; Willmann, Stocker and Dörsam, 2014). Gravure is one of the backbone technologies of rapidly growing packaging markets and food technology (Siever, 2019) in numerous upcoming economies of the eastern hemisphere. In view of the present global economic and ecological challenges, recent developments in gravure technology, namely those obtained from printed electronics applications, could be useful to further reduce the quantities of printing material per area, to minimize the quantities of ecologically hazardous solvents, and to process increasingly complex functional inks. From the printer's point of view, the processing demands of extremely thin, closed layers of highly developed functional polymers or of nanoparticle colloids are not that much different from printing organic solar cells, or light emitting diodes. Both are, admittedly, at the very high edge of present gravure technology. Nevertheless, the manufacturing of closed and smooth polymer layers of only few tens of nanometres in thickness has become a standard task in organic light emitting diode (OLED) printing (Grau, et al., 2016; Kopola, et al., 2009). Bornemann (2014) was one of the first to notice the remarkable stability of such processes. He observed that, under particular conditions, the deposition of such extreme layers was successful on elastic foils as well as on rigid and wavy glass substrates at velocities beyond 3 m/s. This was attributed to a specific dynamical and stable regime of the ink splitting or cell emptying process in the nip. The physical origin of this somewhat exceptional process and closer hydrodynamic details of ink flow remained obscure at that time. The resolution of this point was recognized much later, using high-speed video recording of the nip as done by Griesheimer (2014); Sauer, et al. (2018), and, in particular, by Schäfer, et al. (2019). Studying the hydrodynamics at a millisecond time scale on mesoscopically structured surfaces provides surprising transient cell emptying flow phenomena,

correlated on length scales of few gravure raster distances. In contrast to point and lamella splitting, there is up to now no scheme to distinguish the residuals of these transient flows in the printed pattern after leaving the nip. This is the concern of our paper.

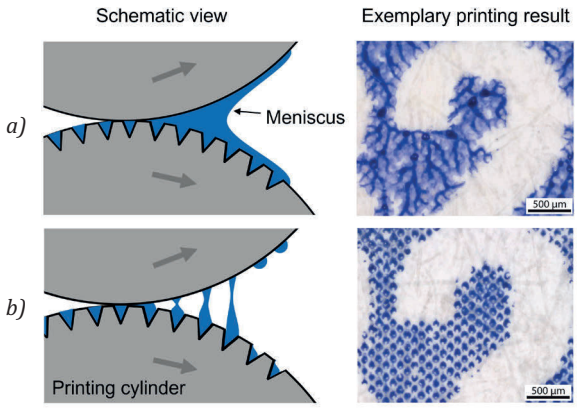

Figure 1: Schematic view of (a) lamella splitting (class 1), and (b) point splitting (class 2), in gravure printing

On the phenomenological level, according to Hübner (1991), one can distinguish two classes of ink splitting: *lamella splitting* (class 1) and *point splitting* (class 2), as shown in Figure 1. Point splitting implies that each gravure cell deposits an individual ink drop at the specific target point on the substrate. This creates the well-known raster pattern underlying a gravure printed image. Deviations from regularity are considered as defects, i. e. missing dots (Rong and Pekarovicova, 2007), or point spreading, driven by capillary and substrate imbibition forces. These effects may be also caused by gravure defects on the cylinder, however, they are not considered as the effect of ink capillarity between the diverging surfaces in the nip. The opposite case is referred to as lamella splitting. Ink drops from adjacent cells already coalesce on the printing cylinder. A continuous and highly dynamic fluid meniscus is formed in the nip, and the ink is dragged out of the cells from this meniscus and forms a closed ink layer on the substrate. Clearly, this effect spoils printing resolution. However, the positive aspect is that the considerable capillary energy of the deposited film is counteracted by the dewetting tendencies induced by the substrate. Initially, the liquid layer is metastable and delicate. Stochastic fluctuation phenomena such as *viscous fingering* or Marangoni effects may occur, and initiate e. g. a layer breakdown in the subsequent drying process. The primary goal of printing process and gravure pattern optimization, however, is to bring the liquid film across the first hurdle which is fluid transfer. Providing appropriate conditions for safe leveling of the liquid layer is a subsequent, but largely independent issue as discussed by Sauer, Braig and Dörsam (2020).

In considerable part, our understanding of ink splitting flows has developed from studies on the Hele-Shaw-Cell by Saffman and Taylor (1958) and on forward and reverse gravure roll coating (Gaskell, Savage and Summers, 1996; Benkreira and Cohu, 1998; Gaskell, Innes and Savage, 1998; Schwartz, 1999; Hewson, Kapur and Gaskell, 2006; 2009). Gravure printing is considered as the special case where cylinder and substrate surface are in synchronous motion. This view, at least for moderate printing velocities, has been supported by the work of Hopkins (1957); Kunz (1975); Hübner (1991); Voß (2002); Bornemann (2014), and, concerning flexography, by Hamblyn (2015) and Brumm, Sauer and Dörsam (2019). These studies claim that the ink splitting hydrodynamics is a unique matter of the capillary number of the ink flow in the nip, the ratio of viscous and capillary forces.

Nevertheless, there are parallel observations of ink splitting phenomena in the gravure printing process which cannot be distinguished by capillary numbers alone. Trnovec (2013) has found that pattern formation, at elevated printing velocities, systematically diverges from the expectations of former studies. This was assigned to the Bernoulli pressure under the doctor blade, which affects the filling level of the cells. However, the conclusion is that mass inertia of the ink also becomes relevant, in addition to capillarity and viscous forces. Griesheimer (2014) has demonstrated by his early high-speed video studies that, even in the nip, mass inertia takes over the fluid dynamics in the late phase of ink splitting, when liquid filaments and sheets are evolving in the ink splitting process. Gravure printing hydrodynamics becomes more 'inkjet'-like. The observed effects depend on the Laplace or, equivalently, on the Ohnesorge number.

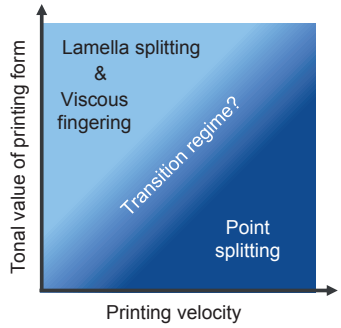

Figure 2: Qualitative concept of the transition between point splitting and lamella splitting

A first qualitative concept on transition between point and lamella splitting is depicted in Figure 2. With increasing printing velocity and decreasing raster cell volume per surface area, which equals decreasing tonal values, ink splitting dynamics will toggle between lamella and point splitting. We focus on the parame-

ter regime close to this transition. We want to know if there is a transition area or a clear separation into point splitting and lamella splitting.

In a sequence of gravure printing experiments, we have elucidated the pattern formation phenomenology of the ink splitting process. After having identified the parameter ranges where the transition regime is located, our study on pattern formation was focussed on the effect of small parameter changes on pattern formation. Careful parameter variation should show that the transition may have an intermediate regime which cannot be assigned to the traditional two-class distinction.

2. Materials and methods

2.1 Printing experiments

For our experiments, we used a lab-scale sheet-fed gravure printer (GT+W Superproofer 220, Rödermark, Germany), which was also described in (Schäfer, Sauer and Dörsam, 2018; Schäfer, et al., 2019). The speciality of the setup used as shown in Figure 3 is a substrate carrier on which the substrate is mounted on the bottom side. The carrier is then accelerated by a linear motor to move the substrate into the printing nip and therefore across the gravure cylinder, with specified printing velocity (20–300 m/min). With such a setup only small amounts of ink (1–3 ml) are needed for the experiment.

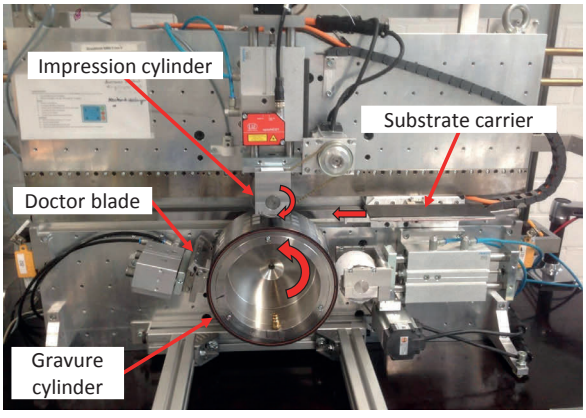

Figure 3: Gravure printing setup

Table 1 shows the parameter combinations used for the printing experiments. We used printing velocities of {20, 30, 45, 60, 75, 90, 160} m/min. As printing fluids, we utilized water-based gravure inks in a red (SunChemical R0001235761) and a blue (SunChemical B0001117761) version. In addition, a diluted version of the red ink (10.14 g of printing ink with 9 g of distilled water) was tested.

Table 1: Parameter combinations used in the printing experiments (the exact names of all inks and substrates can be found in the text in Section 2.1)

Parameter combination	Printing velocity in m/min	Printing fluid	Substrate
1	20	Red ink	Paper
2	30	Red ink	Paper
3	45	Red ink	Paper
4	60	Red ink	Paper
5	75	Red ink	Paper
6	90	Red ink	Paper
7	160	Red ink	Paper
8	30	Red ink	Foil
9	30	Diluted red ink	Paper
10	30	Blue ink	Paper

As substrates, we used paper (UPM Finesse matte-coated H) with a grammage of 100 g/m^2 and coated transparent foil (Hostaphan® GN 4660A) with a thickness of 125 µm. Substrates were cut to 200 mm × 60 mm and attached to the substrate carrier. Doctor blade pressure and angle, and also nip pressure are given in Table 2. The machine was operated in a climatized, filtered atmosphere at a temperature of 20 ± 2 °C, and a relative humidity of 33 ± 3 %.

Table 2: Process parameters that were kept constant for all printing experiments

Parameter	Value
Doctor blade pressure	0.4 N/mm
Doctor blade angle	60°
Nip pressure	16 N/mm

As printing form, an electromechanically engraved chromium-plated copper sleeve, with stylus angle 120°, raster angle 45°, diameter 220 mm and printing width 100 mm was used (engraver: Sächsische Walzengravur GmbH, Germany). Figure 4 illustrates the relevant parameters of the printing form, which can also be applied to describe the printed product. A 'raster cell' as shown in Figure 4a corresponds to a later printed dot ('raster dot') of the printed product as shown in Figure 4b. Printed dots differ a lot in shape and size. Section A-A shows a sectional view of a single pyramid-shape raster cell of a gravure printing form.

The gravure pattern on the sleeve consisted of five segments distributed over its circumference. Each segment contained two clusters of gravure fields, with specific raster frequencies for each cluster: {40, 48, 54, 60, 70, 80, 90, 100, 120, 140} lines per centimeter (L/cm). Each cluster contained 12 fields of size 13 mm × 13 mm. The tonal values of the fields within each cluster were {5, 10, 20, 30, 40, 50, 60, 70, 80, 90, 95, 100} %. For each

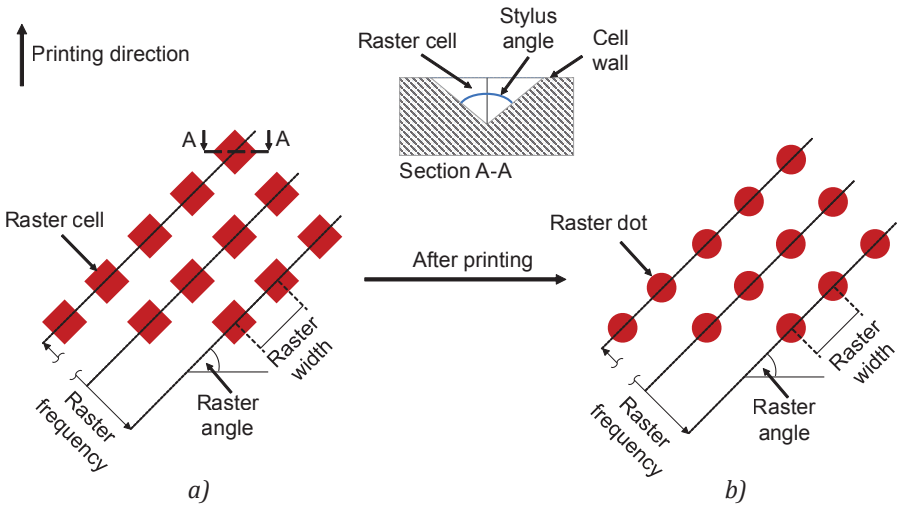

Figure 4: Illustration of (a) relevant parameters of an electromechanically engraved printing form, and (b) the corresponding printed raster pattern

parameter combination in Table 1, all five segments of the printing form were employed for printing in at least three subsequent printing runs. Printing samples from over 3 600 fields (ten parameter combinations × five segments × two clusters × twelve fields × three samples) on over 150 samples were created in this way.

2.2 Classification of the printed samples

2.2.1 Sample digitization

The printed samples were digitized using a flatbed scanner (EPSON Perfection V800 Photo) that was color-calibrated with a Kodak IT8 target once a day before each scanning series. We chose 2 400 dots per inch (dpi) as the nominal scanning resolution. The actual scanning resolution was determined as 1 825 dpi using an USAF-1951 resolution target. Using the professional scanning software SilverFast Ai Studio 8, unfiltered raw data in uncompressed 16 bit RGB TIFF format was created. The size of a digitized sample was about 5 800 × 18 000 pixels. Figure 5 shows such a sample with annotations. The printed fields were 13 mm × 13 mm in size, each with its tonal values in % noted below. Each cluster of 12 fields had a different raster frequency; e. g., cluster 1 had 140 L/cm, cluster 2 had 40 L/cm. The printing direction is given by an arrow. The tail of the arrow indicates areas which were printed earlier in time whereas the arrowhead points towards areas which were printed later in time. The printing parameters for Figure 5 can be looked up in the Appendix in Table A1 where a collection of printing parameters for fields used as examples in Figures 5 to 14 can be found.

All digitized printed fields can be downloaded from <https://doi.org/10.48328/tudatalib-528.2>.

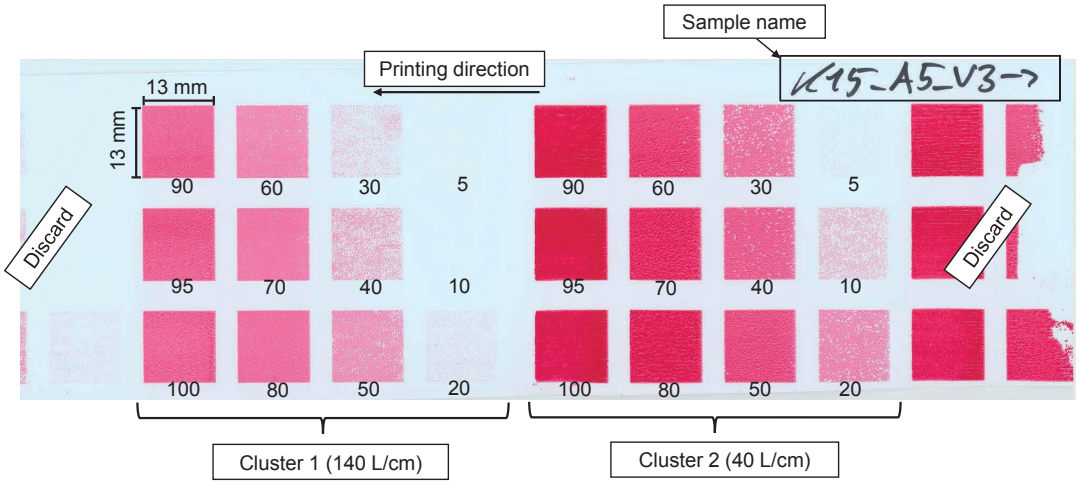

Figure 5: Exemplary digitized sample with annotations

2.2.2 Classification method

We defined criteria to classify each printed field into one of the following three classes: *Lamella splitting* (class 1), *point splitting* (class 2) and *transition regime* (class 3). The criteria for all three classes are indicated in Table 3.

Table 3: Iteratively developed ink splitting classification

Name	Type of ink splitting	Criteria
Class 1	Lamella splitting	There are only *fingers* visible on the field. They can differ in shape, size and orientation. If a form cannot be further discriminated into *dots*, it is seen as a *finger*. There is no single *dot* to be seen.
Class 2	Point splitting	There are only *dots* visible on the field. The *dots* can have different shapes (diamond-, donut-, boomerang-shape, etc.). Connections between *dots* are allowed as long as the *dots* are still discriminable. There is no single *finger* to be seen.
Class 3	Transition regime	There are *dots* as well as *fingers* visible on the field.

In order to apply Table 3, a classification scheme for *dots* and *fingers* was necessary. The graphical classification scheme for dots and fingers with corresponding printing examples is shown in Figure 6. In the classification scheme (top), red areas represent areas wetted with printing ink. The darker the red color the higher the amount of ink. The distance between the dots equals the raster width. The printing examples (bottom) show independent dots (a1.1 to a1.3), connected but still discriminable dots (a2.1), shapes, which cannot further be discriminated into single dots and are therefore considered as fingers (b1.1 and b1.2), and fingers with a *brim* (b2.1 to b2.3). The printing parameters for the printing examples in Figure 6 can be found in the Appendix. In addition to the graphical classification scheme, we provide a textual classification scheme for *dots*, *fingers* and *brim*, as given in Table 4.

Table 4: Textual classification scheme for the terms dot, finger and brim as used in this research

Term	Definition
Dot	Isolated droplet on the printing product on a raster dot position.
Finger	Liquid ink bridge resulting from viscous fingering on the printed product. We assumed that the smallest finger is as long as the distance between two neighbouring raster dots. A finger may be surrounded by a brim.
Brim	Area, which has been in contact with ink intermediately, but now is essentially void of deposited ink, e. g. by dewetting, contact line recession or imbibition. It does not need to be restricted to a certain area but can also cover the whole background of the fingers.

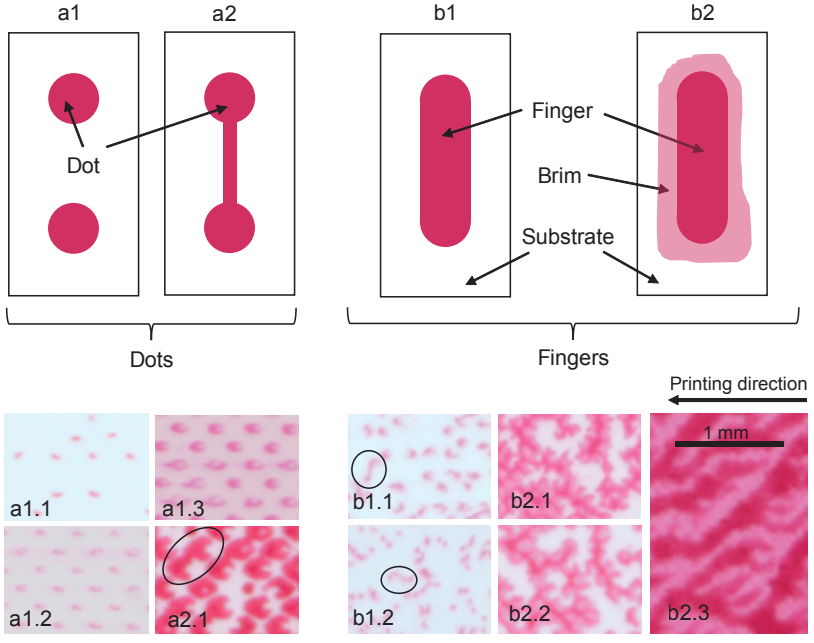

Figure 6: Graphical classification scheme for dots, fingers and brim (top) and corresponding exemplary printed samples (bottom)

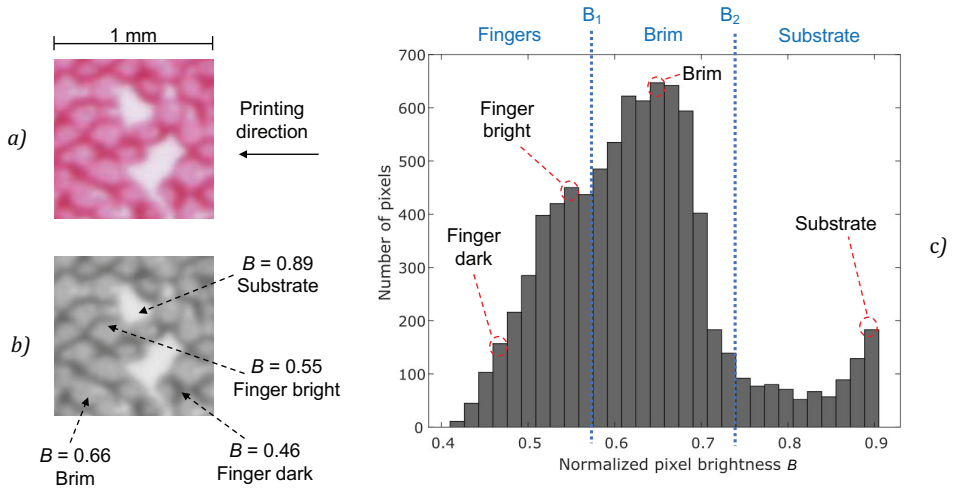

Figure 7: Possible quantitative classification approach to visualize the frequency distribution of brightness values of a sample cut-out (a), converted into grayscale (b), by using a histogram (c)

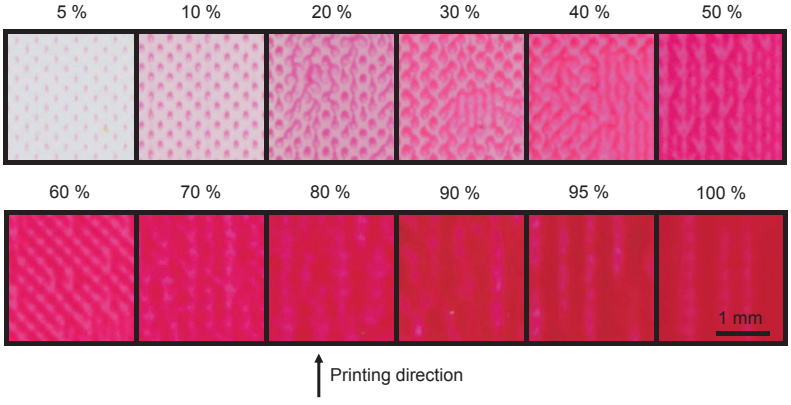

Figure 8: Change of pattern formation by altering the tonal value

In this research, the delicate distinction between dots and substrate or between finger, brim and substrate is done by a (subjective) human observer. As a future quantitative approach, we suggest distinguishing these features using a histogram which shows the frequency distribution of brightness values in a sample image. With certain defined brightness thresholds, fingers, brim and substrate could be distinguished. These brightness thresholds could be identified iteratively or using machine learning approaches for a large number of samples. The proposed quantitative approach is shown exemplarily for a cut-out of one printed field in Figure 7. The RGB sample cut-out (Figure 7a) is converted into grayscale (Figure 7b) and then a histogram with 30 bins is created (Figure 7c). The printing parameters for the printed field in Figure 7 can be found in the Appendix. By looking at the histogram we were at least able to clearly distinguish fingers and brim from the substrate. However, we were not able to easily differentiate brim and fingers since their brightness values are not clearly separated as two separate sharp peaks in the histogram. Rather, brightness values of fingers (dark and bright) and brim merge in one single wide peak in the histogram. Nevertheless, the human observer is able to distinguish fingers and brim, although in a subjective manner. The histogram proves a possible quantitative differentiation of fingers, brim and substrate by defining suitable threshold brightness values B1 and B2, which are chosen exemplarily here. There might be possible disruptive factors for a human observer, e. g. a residual lubrication film from the doctor blading process on the substrate or the phenomenon of dot gain which need to be distinguished from the expected features (dots, fingers, brim, substrate). These disruptive features have to be taken into account when developing a future objective classification approach.

Figure 8 exemplarily illustrates the transition from low to high tonal values and its resulting development of different patterns. Although each printed sample differs due to its stochastic nature, dots can be found at

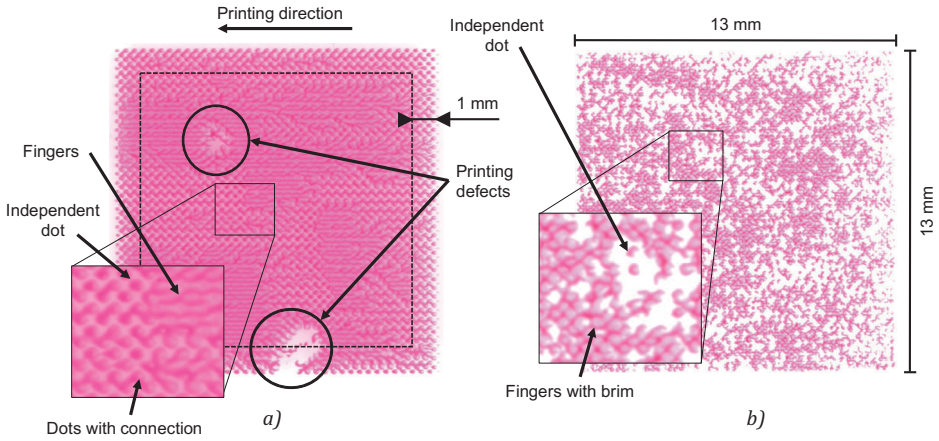

Figure 9: Transition regime, as seen on two fields (a) and (b)

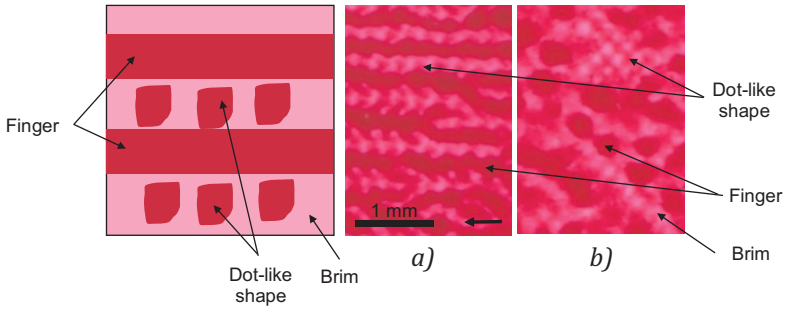

Figure 10: Dot-like shapes next to fingers as observed on two different fields (a) and (b), which are classified as lamella splitting

lower tonal values while finger patterns can be seen at higher tonal values. The transition regime in this example is located at tonal values of 20 %, 30 % and 40 %. The printing parameters used to create the various kinds of patterns in Figure 8 can be found in the Appendix.

All digitized samples with over 3 600 fields were visually examined on a computer screen using adequate digital magnification. We assigned one of the three classes in Table 3 to each field. Obvious printing defects were always excluded from visual assessment as well as the rim of the fields (about 1 mm from each edge towards the center of the field), since it showed different pattern formation than the inside of the fields (Figure 9). We assume that only the inside of the fields exhibits stationary pattern formation phenomena. Figure 9 shows typical examples for the transition regime on foil (Figure 9a) and on paper (Figure 9b). In the fields classified as transition regime, dots as well as fingers appear. The printing parameters used to print the two fields in Figure 9 can be found in the Appendix.

Within the classification process, we found an especially interesting but complex type of pattern formation as seen in Figure 10 on two different fields (Figure 10a and Figure 10b). Printing parameters can be found in the Appendix. Both fields show a pattern of dot-like shapes located on the brim next to fully developed fingers. The arrow indicates the printing direction. Since the dot-like shapes show up with a brim, they do not fall under our definition of dots. Therefore, the patterns in Figure 10 were not assigned to the class of transition regime (class 3). In fact, they were assigned to the class of lamella splitting (class 2) in this research, because there are only fingers and no dots visible on the fields, compare with Table 3. Further investigation is needed to explain the existence of dot-like shapes near to fully developed fingers. We assume that this phenomenon could be related to the absorbing properties of paper substrates, which preserves former states of forced wetting during the gravure printing process.

3. Results and discussion

Figure 11 shows classification results for red ink on paper for ten different raster frequencies: {40, 48, 54, 60, 70, 80, 90, 100, 120, 140} L/cm. On the horizontal axis, we show the printing velocity and on the vertical axis, the tonal value (left) as well as the raster frequency (right). We marked the upper and lower bor-

ders of the transition regime, by plotting the last field classified as point splitting and the first field classified as lamella splitting in a series of fields with increasing tonal values. The lines between the data points are linear interpolations. The three regimes lamella splitting, point splitting and transition regime are marked with different infill colors as shown in the legend in Figure 11. Each data point represents the combined classification result of at least three samples with the same parameter combination. For example, when we classified a field two times as transition regime and once as lamella splitting, transition regime was chosen. We expect the lamella splitting, the point splitting and the transition regime to be continuous and clearly separated. Thus, we were able to detect and exclude outliers from our data, e. g. a point splitting field in the lamella splitting regime which was caused by too little ink being transferred (obvious printing defect).

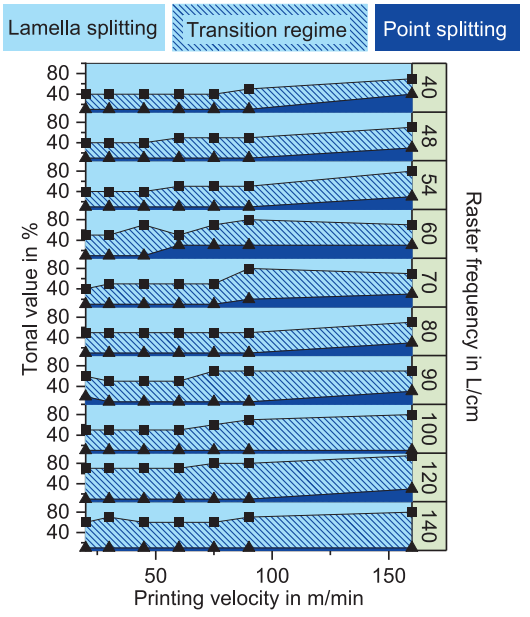

Figure 11: Classification results for the samples printed with red ink on paper

For better visualisation, the classification results shown in Figure 11 were combined in one single diagram (Figure 12) by averaging of all data points from all raster frequencies and subsequent linear interpolation to obtain the regime borders. Figure 12 shows printing velocity on the horizontal axis and tonal value on the vertical axis. It displays the regimes of printing velocity and tonal value, where lamella splitting, point splitting and an intermediate regime (the transition regime) were observed. With higher printing velocities, the transition regime shifts to higher tonal values. We observe lamella splitting at higher tonal values and point splitting at lower tonal values. This finding is in good agreement with literature, which says that the amount of ink is rather high for lamella splitting and rather low for point splitting (Hübner, 1991). Furthermore, we observed that for tonal values of 10 % and lower, only point splitting occurs. From Figure 12 we can derive linear trend lines for the regime borders, as marked in red dashed and dashed-dotted lines. The linear trend lines for the upper and lower regime borders are given as $y = 43.2 + 0.2x$ (red dashed line) and $y = 4.5 + 0.1x$ (red dash-dotted line), respectively, where y is the tonal value in % and x is the printing velocity in m/min.

Figure 12 shows that the size of the transition regime is unexpectedly large in comparison to the point splitting regime and even about as large as the lamella splitting regime. We assume that this has three possible reasons. First, the use of a paper substrate which causes relatively many printing defects. Second, the harsh criteria for the classification as transition regime, as chosen for this research. And third, our way of representing the regime map.

To start with the first reason, paper is a rather rough substrate (compared to foil) and thus most of the printed samples show relatively many missing dots or other printing defects. These printing defects (if not evaluated as obvious printing defects and therefore excluded by the human observer) can lead to classifying a field as transition regime since a printing defect might look like a dot in a field of fingers only.

According to the developed classification scheme from Table 3, one single dot in a field with only fingers is responsible for the classification as transition regime. This is reason two for the large transition regime. For future research, we suggest softening this relatively harsh criterion for the benefit of the robustness of our approach. For example, the existence of five dots in a field of fingers only could lead to the classification as transition regime. For the manual assessment by a human observer, a threshold of five dots would have led to an exponentially higher expenditure of time for classification which would have not been feasible. When using quantitative, automated classification approaches, e. g. image processing with deterministic algorithms or machine learning approaches, the choice of arbitrary thresholds would become feasible.

The third reason for the large transition regime is the way of representing the regime map. We chose to mark the last field that exhibits point splitting and the first field that exhibits lamella splitting in a series of increasing tonal values. Since we have discrete tonal values in 5 % or 10 % steps, the transition regime seems larger in the negative and positive y-direction up to one step. For example, when tonal values {5, 10} % are classified as point splitting, {20, 30, 40} % as transition regime and {50, 60, 70 80, 90, 95, 100} % as lamella splitting,

see Figure 8. In this case, we marked 10 % as the lower regime border and 50 % as the upper regime border in the regime map. Alternatively, we could mark the first (20 %) and the last field (40 %) that was classified as transition regime, which would lead to a transition regime that appears smaller, but this is not a useful representation when no transition regime exists.

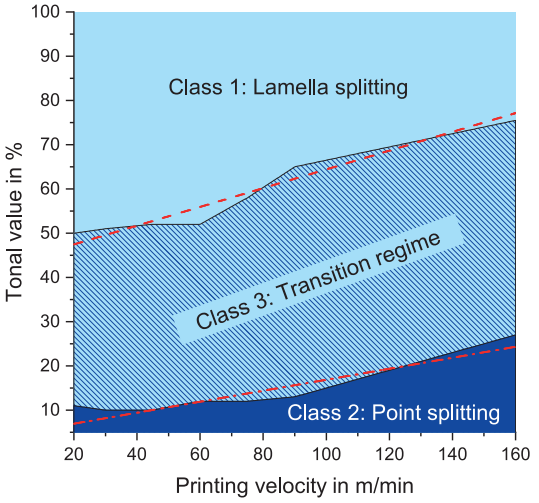

Figure 12: Location of the transition regime for the samples printed with red ink on paper

Substrate and fluid had significant influence on the visual appearance of the samples, particularly on finger shape and size, see Figure 13. Printing parameters can be found in the Appendix. The finger pattern was much less branched on foil than on paper substrates. Finger patterns from red and blue gravure ink did not exhibit a significantly different optical appearance, except that the finger patterns were unique due to their stochastic nature (Fernandes, 2019). Diluted ink showed patterns that looked more washed-out than patterns created with non-diluted ink.

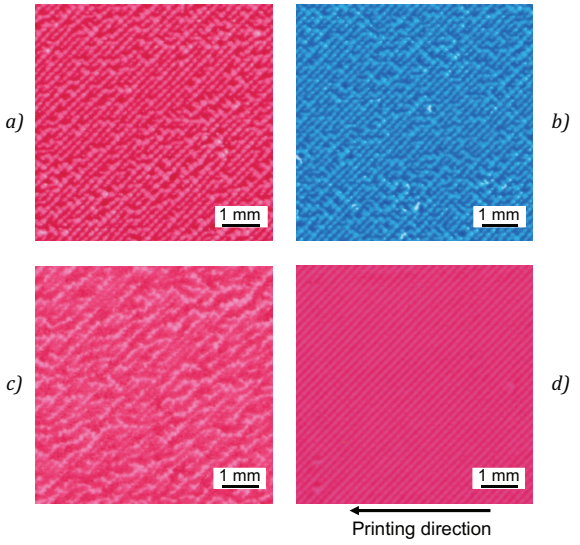

Figure 13: Comparison of pattern formation using (a) red ink on paper, (b) blue ink on paper, (c) water diluted red ink on paper and (d) red ink on foil

According to literature, viscous fingering has its predominant direction parallel to the printing direction. In this research, we also found predominant directions diagonal to the printing direction, see Figure 14. The arrows indicate the printing direction. Printing parameters can be found in the Appendix. Different predominant directions can be observed on the same sample at different tonal values (Figure 14a) or on different samples (Figures 14b to 14e). There can also be found several predominant directions in one and the same printed field, e. g. Figure 14e.

In summary, we have found evidence for the possibility of more complex types of ink splitting in the gravure process. With our classification scheme, we were able to localize the point and lamella splitting regimes as well as the transition regime. Our findings may serve

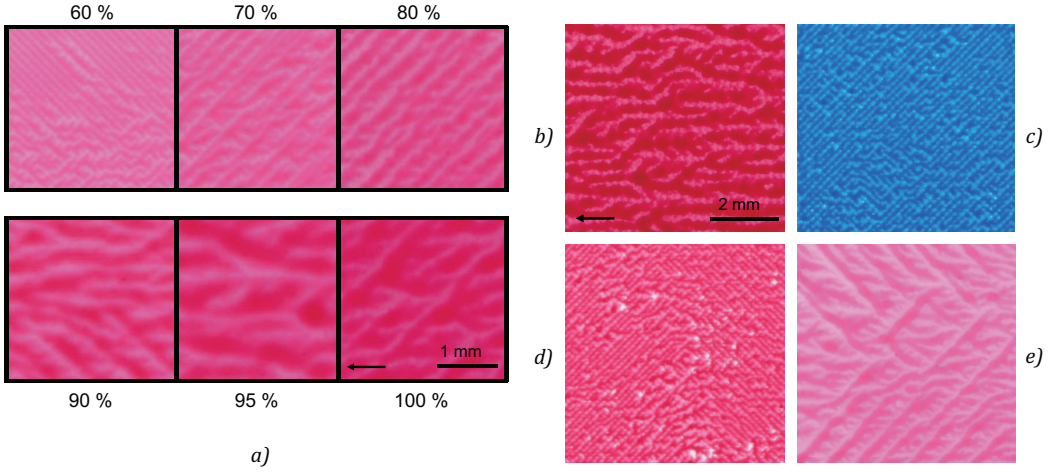

Figure 14: Various predominant directions of finger patterns, not only parallel but also diagonal to the printing direction, can be observed (a) on the same sample at different tonal values, and (b–e) on different samples

as a guideline for practical application. We emphasize that, depending on printing parameters, ink splitting in the transition regime may exhibit different types of pattern formation that we were not able to resolve here.

4. Conclusions and outlook

As shown in Sections 2 and 3 we were able to create a common basis for the classification of point and lamella splitting, and the intermediate transition regime. We were able to create a classification scheme for the three regimes, by evaluating data from over 3 600 printed fields. Moreover, we were able to come up with an empirical assessment of tonal value vs. printing velocity and the impact of both on the creation of the three mentioned regimes. With this, our classification scheme sets the basis for further investigations on the transition from point to lamella splitting. However, the developed method is still at an early stage. Visual assessment and classification into dots and fingers depends on the subjective judgement of a human observer and on conditions of visual inspection. Thus, a precise classification of the morphologies is required which goes beyond the binary distinction of point and lamella splitting. Our aim here was to show that such a classification is feasible. Our findings on ink splitting contribute to known results by a refinement of the common picture. It must be noted that the distinction into the three classes as mentioned above might not capture the full spectrum of patterns and transition effects and thus is subject to further research. There is reason to suspect that even more distinctions are necessary, yielding interesting process options for novel applications of gravure printing e. g. security features or functional coating with only partial percentage of ink covering.

Optical resolution clearly is a limitation of our approach, although our definition of dots and fingers also works for higher resolutions. At high raster frequencies, e. g. 140 L/cm, the printed dots were so small that scanning resolution was at its limit. At this limit of resolution, the distinction between dot and finger is rather subjective. Another limitation is the fact that we examine the printed sample after drying. This means that the sub-steps of ink relaxation and drying on the substrate, which occur after fluid transfer, have an impact on the result. Nevertheless, for this research, we assume that the printed sample is a frozen image of the moment right after fluid transfer.

For future research, in-situ experiments with high-speed imaging of ink splitting like in Schäfer, et al. (2019) are promising. In-situ experiments are elaborate, but provide more complex insight compared to our ex-situ experiments (using the printed products as samples), which are comparatively simple to implement and thus more user-friendly. For our approach, just a gravure printing machine, a high-resolution scanner, a computer for image observation and an instructed human observer are needed. For in-situ experiments, generally, expensive high-speed imaging equipment, a modified, optically accessible gravure printing machine and software for automated image analysis are needed. For future research, digital image processing, computer vision and machine learning algorithms for pattern recognition could be used in order to increase objectivity of the developed classification approach. For example, frequency-based image analysis using Fast Fourier Transformation as described in Brumm, Sauer and Dörsam (2019) could be used to determine the dominant pattern frequency and thus clearly differentiate between dominant finger frequency and known raster dot frequency. This could help in distinguishing dots and fingers. Moreover, scaling laws of finger formation can be obtained. Using more objective and automated approaches, the upscaling of gravure printing process research to industrial scale could be promoted. For future research, we plan to conduct gravure printing experiments at industrial scale and at higher printing velocities and compare the results to this research.

Acknowledgments

We kindly acknowledge the financial support by the Deutsche Forschungsgemeinschaft (DFG, German Research Foundation) – Project-ID 265191195 – SFB 1194 'Interaction between Transport and Wetting Processes', project C01. Besides, we kindly thank Thorsten Euler for his help in operating the printing machine.

References

Benkreira, H. and Cohu, O., 1998. Direct forward gravure coating on unsupported web. *Chemical Engineering Science,* 53(6), pp. 1223–1231. https://doi.org/10.1016/S0009-2509(97)00446-6.

Bornemann, N., 2014. *Characterization and investigation of large-area, ultra-thin gravure printed layers*. Doctoral thesis. Technische Universität Darmstadt. [online] Available at: <https://tuprints.ulb.tu-darmstadt.de/id/eprint/3847> [Accessed 29 November 2020].

Brumm, P., Sauer, H.M. and Dörsam, E., 2019. Scaling behavior of pattern formation in the flexographic ink splitting process. *Colloids and Interfaces,* 3(1): 37. https://doi.org/10.3390/colloids3010037.

Fernandes, F.C., 2019. *Entwicklung von gedruckten stochastischen Identifikationsmerkmalen.* Doctoral thesis. Technische Universität Darmstadt. [online] Available at: <https://tuprints.ulb.tu-darmstadt.de/id/eprint/8795> [Accessed 29 November 2020].

Ganz, S., Sauer, H.M., Weißenseel, S., Zembron, J., Tone, R., Dörsam, E., Schaefer, M. and Schulz-Ruthenberg, M., 2016. Printing and Processing Techniques. In: G. Nisato, D. Lupo and S. Ganz, eds. *Organic and printed electronics: fundamentals and applications.* Singapore: Pan Stanford Publishing, pp. 47–116.

Gaskell, P.H., Savage, M.D., and Summers, J.L., eds., 1996. *First European Coating Symposium on the Mechanics of Thin Film Coatings.* Leeds University, UK, 19–22 September 1995. Singapore: World Scientific Publishing. https://doi.org/10.1142/3007.

Gaskell, P.H., Innes, G.E. and Savage, M.D., 1998. An experimental investigation of meniscus roll coating. *Journal of Fluid Mechanics*, 355, pp. 17–44. https://doi.org/10.1017/S0022112097007398.

Grau, G., Cen, J., Kang, H., Kitsomboonloha, R., Scheideler, W.J. and Subramanian, V., 2016. Gravure-printed electronics: recent progress in tooling development, understanding of printing physics, and realization of printed devices. *Flexible and Printed Electronics*, 1(2): 023002. https://doi.org/10.1088/2058-8585/1/2/023002.

Griesheimer, S., 2014. *Farbspaltungsphänomene von Druckfarben an strukturierten Oberflächen am Beispiel des Flexodrucks*. Doctoral thesis. Technische Universität Darmstadt.
[online] Available at: <https://tuprints.ulb.tu-darmstadt.de/id/eprint/3892> [Accessed 29 November 2020].

Hamblyn, A., 2015. *Effect of plate characteristics on ink transfer in flexographic printing*. Doctoral thesis. Swansea University. [online] Available at: <https://cronfa.swan.ac.uk/Record/cronfa42827> [Accessed 29 November 2020].

Hewson, R.W., Kapur, N. and Gaskell, P.H., 2006. A theoretical and experimental investigation of tri-helical gravure roll coating. *Chemical Engineering Science*, 61(16), pp. 5487–5499. https://doi.org/10.1016/j.ces.2006.04.021.

Hewson, R.W., Kapur, N. and Gaskell, P.H., 2009. Modelling the discrete-cell gravure roll coating process. *The European Physical Journal Special Topics*, 166, pp. 99–102. https://doi.org/10.1140/epjst/e2009-00886-x.

Hopkins, M.R., 1957. Viscous flow between rotating cylinders and a sheet moving between them. *British Journal of Applied Physics*, 8(11), pp. 442–444. https://doi.org/10.1088/0508-3443/8/11/303.

Hübner, G., 1991. *Ein Beitrag zum Problem der Flüssigkeitsspaltung in der Drucktechnik*. Doctoral thesis. Technische Universität Darmstadt. https://doi.org/10.25534/tuprints-00013550.

Kopola, P., Tuomikoski, M., Suhonen, R. and Maaninen, A., 2009. Gravure printed organic light emitting diodes for lighting applications. *Thin Solid Films*, 517(19), pp. 5757–5762. https://doi.org/10.1016/j.tsf.2009.03.209.

Kumar, S., 2015. Liquid transfer in printing processes: liquid bridges with moving contact lines. *Annual Review of Fluid Mechanics*, 47(1), pp. 67–94. https://doi.org/10.1146/annurev-fluid-010814-014620.

Kunz, W., 1975. Ink transfer in gravure process. In: *TAGA Proceedings 1975: Annual meeting of the Technical Association of the Graphic Arts.* Toronto, Ontario, 1975. Rochester, NY, USA: TAGA, pp. 151–176.

Rong, X. and Pekarovicova, A., 2007. The study of missing dots of electromechanical and laser engraved cylinders. In: *TAGA Proceedings 2007: Annual meeting of the Technical Association of the Graphic Arts*. Pittsburgh, PA, USA, 18–21 March 2007. Sewickley, PA, USA: TAGA, pp. 596–604.

Saffman, P.G. and Taylor, G.I., 1958. The penetration of a fluid into a porous medium or Hele-Shaw cell containing a more viscous liquid. *Proceedings of the Royal Society A: Mathematical, Physical and Engineering Sciences*, 245(1242), pp. 312–329. https://doi.org/10.1098/rspa.1958.0085.

Sauer, H.M., Braig, F. and Dörsam, E., 2020. Leveling and drying dynamics of printed liquid films of organic semiconductor solutions in OLED/OPV applications. *Advanced Materials Technologies*, 6(2): 2000160. https://doi.org/10.1002/admt.202000160.

Sauer, H.M., Roisman, I.V., Dörsam, E. and Tropea, C., 2018. Fast liquid sheet and filament dynamics in the fluid splitting process. *Colloids and Surfaces A: Physicochemical and Engineering Aspects*, 557, pp. 20–27. https://doi.org/10.1016/j.colsurfa.2018.05.101.

Schäfer, J., Sauer, H.M. and Dörsam, E., 2018. Direct observation of high-speed fluid transfer phenomena in the nip of a gravure printing machine. In: P. Gane, ed. *Advances in Printing and Media Technology Vol. XLV(V): Proceedings of the 45th International Research Conference of iarigai*, Warsaw, Poland, October 2018. Darmstadt, Germany: iarigai, pp. 72–81.

Schäfer, J., Roisman, I.V., Sauer, H.M. and Dörsam, E., 2019. Millisecond fluid pattern formation in the nip of a gravure printing machine. *Colloids and Surfaces A: Physicochemical and Engineering Aspects,* 575, pp. 222–229. https://doi.org/10.1016/j.colsurfa.2019.04.085.

Schwartz, L.W., 1999. Theoretical and numerical modelling of coating flow on simple and complex substrates including rheology, drying and Marangoni effects. In: F. Durst and H. Raszillier, eds. *European Coating Symposium: Advances in Coating and Drying of Thin Films*. Erlangen, Germany. Aachen: Shaker Verlag, pp. 105–128.

Siever, J., 2019. Gravure market in Pakistan. *Gravure News,* 183(1), pp. 4–7.

Trnovec, B., 2013. *Experimentelle Untersuchungen zur Schichtbildung im Tiefdruck mittels hydrophobierter Druckform mit Applikationsbeispielen aus dem Bereich der gedruckten OPV*. Doctoral thesis. Technische Universität Chemnitz. [online] Available at: <https://nbn-resolving.org/urn:nbn:de:bsz:ch1-qucosa-209748> [Accessed 29 November 2020].

Voß, C., 2002. *Analytische Modellierung, experimentelle Untersuchungen und dreidimensionale Gitter-Boltzmann Simulation der quasistatischen und instabilen Farbspaltung*. Doctoral thesis. Bergische Universität Gesamthochschule Wuppertal. Available at: <https://nbn-resolving.org/urn:nbn:de:hbz:468-20020367> [Accessed 29 November 2020].

Willmann, J., Stocker, D. and Dörsam, E., 2014. Characteristics and evaluation criteria of substrate-based manufacturing. Is roll-to-roll the best solution for printed electronics? *Organic Electronics*, 15(7), pp. 1631–1640. https://doi.org/10.1016/j.orgel.2014.04.022.

Appendix

Printing parameters introduced in Figures 5 to 14 are shown in Table A1.

Table A1: Collection of printing parameters of printed fields used as examples in Figures 5 to 14

Figure number	Suffix	Raster frequency in L/cm	Tonal value in %	Printing velocity in m/min	Fluid	Substrate
5	–	40, 140	5–100	45	Red ink	Paper
6	a1.1	40	5	20	Red ink	Paper
	a1.2	40	5	30	Red ink	Foil
	a1.3	40	10	30	Red ink	Foil
	a2.1	40	40	160	Red ink	Paper
	b1.1	54	20	30	Red ink	Paper
	b1.2	140	20	60	Red ink	Paper
	b2.1	70	30	30	Red ink	Paper
	b2.2	90	50	60	Red ink	Paper
	b2.3	120	95	45	Red ink	Paper
7	–	60	40	30	Red ink	Paper
8	–	40	5–100	30	Red ink	Foil
9	a	40	40	30	Red ink	Foil
	b	60	40	30	Red ink	Paper
10	a	48	95	20	Red ink	Paper
	b	48	90	20	Red ink	Paper
13	a	60	70	30	Red ink	Paper
	b	60	70	30	Blue ink	Paper
	c	60	70	30	Diluted red ink	Paper
	d	60	70	30	Red ink	Foil
14	a	90	60–100	30	Red ink	Foil
	b	54	100	20	Red ink	Paper
	c	48	80	30	Blue ink	Paper
	d	54	60	60	Red ink	Paper
	e	120	90	30	Red ink	Foil